Decoupling of the brain's default mode network during deep sleep

Silvina G. Horovitz[a,b,1], Allen R. Braun[c], Walter S. Carr[d], Dante Picchioni[e], Thomas J. Balkin[e], Masaki Fukunaga[b], and Jeff H. Duyn[b]

[a]Human Motor Control Section, Medical Neurology Branch, National Institute of Neurological Disorders and Stroke, National Institutes of Health, Bethesda, MD 20892; [b]Advanced MRI, Laboratory of Functional and Molecular Imaging, National Institute of Neurological Disorders and Stroke, National Institutes of Health, Bethesda, MD 20892; [c]Language Section, Voice, Speech and Language Branch, National Institute on Deafness and Other Communication Disorders, National Institutes of Health, Bethesda, MD 20892; [d]Naval Medical Research Center, Silver Spring, MD 20910; and [e]Department of Behavioral Biology, Walter Reed Army Institute of Research, Silver Spring, MD 20910

Edited by Leslie G. Ungerleider, National Institute of Health, Bethesda, MD, and approved May 7, 2009 (received for review February 9, 2009)

The recent discovery of a circuit of brain regions that is highly active in the absence of overt behavior has led to a quest for revealing the possible function of this so-called *default-mode network* (DMN). A very recent study, finding similarities in awake humans and anesthetized primates, has suggested that DMN activity might not simply reflect ongoing conscious mentation but rather a more general form of network dynamics typical of complex systems. Here, by performing functional MRI in humans, it is shown that a natural, sleep-induced reduction of consciousness is reflected in altered correlation between DMN network components, most notably a reduced involvement of frontal cortex. This suggests that DMN may play an important role in the sustenance of conscious awareness.

EEG | fMRI | resting state | connectivity | consciousness

All except the most simple reflexive behaviors are mediated by and reflected in the chemical and electrical signaling within the brain's circuitry. The ability to monitor the spatial distribution of such activity with modern neuroimaging techniques such as PET (1) and functional MRI (fMRI) (2) has greatly expanded knowledge of the brain's architecture and functioning, identifying the brain circuitry that underlies a variety of processes and behaviors.

fMRI studies have demonstrated that a substantial level of brain activity also occurs in the absence of overt or task-related behavior (3–8). This spontaneous activity has spatial and temporal characteristics that resemble those of intracortical electrical and optical recordings (9–11). In particular, a network of brain regions has been identified in which activity is actually increased in absence of cognitively demanding tasks (12, 13). This network, termed the *default mode network* (DMN) (14), was initially thought to be associated with conscious, internally mediated cognitive processes—for example, self-referential behavior, moral reasoning, recollection, and imagining the future (14)—cognitive processes thought to be unique to humans. Recent studies have demonstrated that DMN connectivity persists during light sleep (8, 15); however, this persistence could be expected because self-reflective thoughts do not abruptly cease but rather decrease gradually as a person falls asleep, to the point of being virtually absent during the deepest stages of sleep (16).

Adding to these intriguing findings is a recent study of the DMN in anesthetized nonhuman primates (17). Although the general extent of DMN activity was found to be similar to that in awake human, some notable differences can be seen from this study's data [see Fig. 4 in Vincent et al. (17)], including a somewhat reduced spatial involvement of the medial prefrontal cortex. The basis of such differences is not clear and might reflect (*i*) species-specific features/differences in cognitive abilities or (*ii*) alterations in consciousness level due to the effects of the anesthesia.

To clarify these issues, the present study aimed at investigating the relationship between level of consciousness and DMN activity in humans during wakefulness and deep sleep, defined by standard spectral and polysomnographic criteria. Deep sleep is a phase of sleep during which the arousal threshold to external stimuli is maximal (18) and during which the level of consciousness awareness is presumed minimal (16, 19). Thus, the deep-sleep condition allowed strong, ecologically valid modulation of the level of consciousness without resorting to the less-natural conditions of absence seizure, coma, or anesthesia (20).

Similar to previous studies, activity levels were inferred from low-frequency (<0.08 Hz) fMRI signal fluctuation levels, and both coherence and amplitude of activity in the various regional components of the DMN were studied. Sleep level was assessed from concurrently acquired EEG data.

Results

Data Quality. Good quality EEG–fMRI data were collected from 12 of the 18 subjects studied (supporting information Table S1). Of these, 7 experienced at least 15 min of continuous deep sleep required for the analysis. An example of the EEG during the 3-h scan session for a subject is shown in Fig. S1. Sleep structure for the 7 subjects included in the deep-sleep analysis is described in Table S2.

DMN During Wake: Resting-State Network. In a subgroup of volunteers ($n = 5$), we collected resting fMRI, during day hours and without sleep deprivation, using the same imaging parameters. DMN by correlating each voxel's time course with the average time course of the posterior cingulate cortex (PCC) defined according to an anatomic template (21). During wake, the distribution of coherent DMN activity was similar to that described in previous reports (7, 8, 22). Network activity included the seed region and its surroundings (PCC/precuneus [P]), bilateral inferior parietal cortices (IPC) and angular gyri (AG), and frontal regions including medial prefrontal cortex (MPFC) and anterior cingulate cortex (ACC) (Fig. 1*A* and Table 1).

DMN During Deep Sleep. During deep sleep, only partial network involvement was observed, with apparent decoupling of frontal areas from the DMN (Fig. 1*B* and Table 1). Whereas PCC and IPC/AG correlations seem to strengthen, the correlations between PCC and MPFC/ACC became nonsignificant.

Author contributions: S.G.H., A.R.B., W.S.C., D.P., T.J.B., M.F., and J.H.D. designed research; S.G.H., A.R.B., W.S.C., and D.P. performed research; S.G.H. and M.F. contributed new reagents/analytic tools; S.G.H., D.P., and M.F. analyzed data; and S.G.H., A.R.B., W.S.C., D.P., T.J.B., M.F., and J.H.D. wrote the paper.

The authors declare no conflict of interest.

This article is a PNAS Direct Submission.

[1]To whom correspondence should be addressed. E-mail: silvina.horovitz@nih.gov.

This article contains supporting information online at www.pnas.org/cgi/content/full/0901435106/DCSupplemental.

www.pnas.org/cgi/doi/10.1073/pnas.0901435106

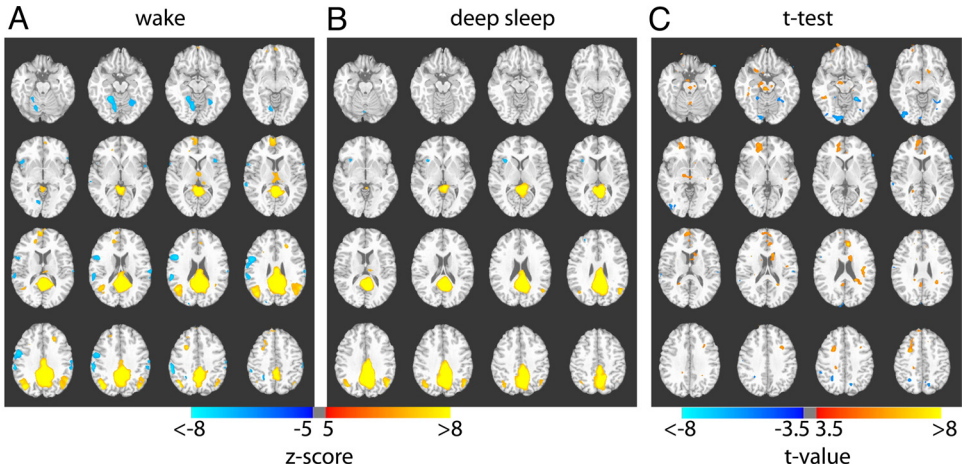

Fig. 1. The default mode network during wake and sleep. Composite maps showing correlations with PCC during (*A*) wake and (*B*) deep sleep, and their significant difference as determined from statistical *t* test (*C*). A significant reduction of involvement of frontal regions is seen during deep sleep, whereas the posterior cingulate–inferior parietal correlations are preserved. The *Z* maps in *A* and *B* are both thresholded at $Z = \pm 5.0$; the *t* map in *C* is thresholded at $t = \pm 3.5$. Both positive (yellow–red) and negative (blue) correlations are shown. *Z* values, *t* values, and Talairach coordinates of all significant clusters are reported in Tables 1 and 2.

Comparison of the DMN in Wake and Deep Sleep. Statistical comparisons of DMN connectivity during wake and deep sleep show a number of differences, most notably in the MPFC/ACC area (Fig. 1*C* and Table 2). Whereas wakefulness was characterized by significant positive correlation between PCC and MPFC/ACC regions, during deep sleep that correlation was absent. Quantitative revealed a significant reduction in the interconnections between the MPFC and other regions during deep sleep. Whereas significant correlations were seen between MPFC and PCC ($r = 0.36$, $P < 0.001$) and all MPFC and right IPC/AG ($r = 0.38$, $P < 0.04$) during the wake state, both became nonsignificant during deep sleep (Fig. 2 and Table 3). The decoupling of frontal and posterior regions during deep sleep was not simply due to reduced frontal activity, given that the amplitude of the fluctuations within that region remained unchanged (Table 4). In fact, robust local coherence of spontaneous activity within all of the component regions of the DMN persisted during deep sleep.

Thus the differences we report are not due to changes in the frontal regions per se. Nor are they due to seed selection: when the seed was placed in the frontal area (Fig. S2) the results were similar to those obtained with the seed in PCC. As with the seed in PCC, seed placement in the frontal region indicated a fully connected DMN in the wake condition (Fig. S2*a*), whereas it led to a dissociation between frontal and parietal areas during deep sleep (Fig. S2*b*). At the same time the correlations within the

Table 1. Center of mass for voxel-by-voxel correlations with PCC seed in wake and deep sleep

Region	Talairach coordinates			Cluster size (mm^3)	Peak *Z* value
	x	y	z		
Wake ($n = 5$)					
Posterior cingulate	−2	−47	23	43,984	31.29
R. angular gyrus	−36	68	33	7,409	9.76
L. angular gyrus	50	56	29	6,763	7.86
R. inferior frontal gyrus	−46	−7	23	4,342	−7.11
R. post-central gyrus	−55	29	38	3,944	−7.21
R. parahippocampal/fusiform	−22	44	−11	3,629	−7.33
Medial frontal gyrus	−6	−61	12	2,920	7.56
L. post-central gyrus	61	21	19	1,992	−5.93
L. post-central gyrus	37	40	60	886	−6.26
L. fusiform	26	55	−10	828	−5.67
R. superior/middle frontal gyrus	−23	−13	39	693	7.05
L. superior/middle frontal gyrus	22	−31	29	498	6.75
Medial frontal/anterior cingulate	−15	−40	18	413	6.45
R. insula	−48	−12	0	325	−5.68
L. insula	36	−17	7	279	−5.72
Medial frontal	0	−57	−5	252	5.59
Deep sleep ($n = 7$)					
Posterior cingulate	−5	−45	23	47,042	23.37
L. angular gyrus	46	64	32	4,014	7.97
R. angular gyrus	−37	66	35	1,941	7.09
R. insula	−31	−17	6	563	−6.45

Threshold $Z = \pm 5$, cluster 250 voxels ($1 \times 1 \times 1$ mm^3).

NEUROSCIENCE

Table 2. Center of mass for voxel-by-voxel *t* test between wake and deep-sleep maps of correlations with PCC seed

Region	Talairach coordinates x	y	z	Cluster size (mm^3)	Peak *t* value
Areas significantly more correlated with PCC during wake (positive *t* values)					
R. medial frontal gyrus/BA10/anterior cingulate	13	49	7	3,413	5.26
R. middle frontal gyrus	24	12	43	1,289	6.67
L. caudate body	−10	8	19	900	5.58
L. anterior cingulate	−5	36	22	881	7.66
L. insula	−39	−20	23	612	5.98
R. red nucleus	3	−25	−14	504	6.04
L. precentral gyrus/middle frontal gyrus	−30	13	35	419	4.66
R. fusiform gyrus	43	−41	−10	353	4.89
R. posterior cingulate	4	−47	25	325	4.72
R. inferior frontal gyrus	24	13	−13	262	4.68
Areas significantly more correlated with PCC during deep sleep (negative *t* values)					
L. fusiform gyrus/parahippocampal gyrus	−27	−52	−8	1200	−8.29
R. lingual gyrus	14	−85	−10	1122	−6.38
R. inferior occipital gyrus	38	−78	−4	930	−6.67
R. pre-central gyrus/BA4	33	−27	57	641	−6.60
R. precuneus/angular gyrus	27	−53	40	472	−4.27
L. precuneus	−13	−65	42	270	−4.68

Threshold $t = \pm 3.5$, cluster 250 voxels ($1 \times 1 \times 1$ mm^3).

frontal region did not change between wake and deep sleep ($t = 2.00$, $P = 0.072$); however, the correlations between MPFC and PCC region decreased from an average of 0.27 during wake to −0.07 during deep sleep ($t = 5.01$, $P = 0.0005$) (Fig. S2*c*).

Temporal Evolution of DMN Activity. The changes in connectivity at different levels of consciousness could also be observed at the individual subject level. For a subject from whom we collected 3 h of data, we evaluated the evolution of the correlation coefficients over time (Fig. 3 and Fig. S3). By correlating the time course of the PCC seed with the whole brain for consecutive 200-point intervals (10 min), we obtained 17 correlation coefficients. These values were compared with the changes in delta power, as reflected by the EEG data, which is itself negatively correlated with arousability. In this subject, the strength of the correlations within the PCC, and between PCC and bilateral IPC, increased as sleep depth increased (correlations between strength of correlations in fMRI and changes in the sleep stage were $r_{pcc/pcc\text{-}sleep\_level} = 0.82$ $r_{pcc/ipl\text{-}sleep\_level} = 0.53$ $r_{pcc/ipr\text{-}sleep\_level} = 0.58$). In contrast, the correlations between PCC and the frontal regions decreased as sleep deepened (correlations between strength of correlations in fMRI and changes in the sleep stage were $r_{pcc/acc\text{-}sleep\_level} = -0.74$ $r_{pcc/mf\text{-}sleep\_level} = -0.80$).

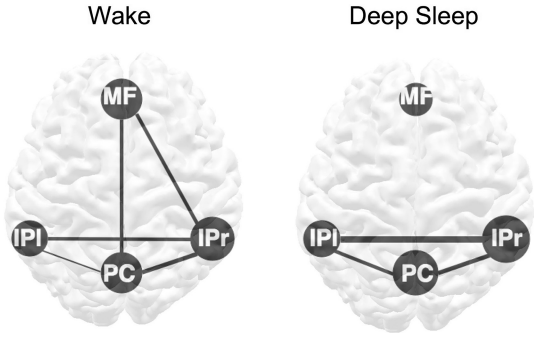

Fig. 2. Connectivity of the main components of the DMN during wake and deep sleep. The connectivity within (disks) and between components (lines) was determined from temporal correlation analysis of average time courses within each ROI. The ROIs were defined as the voxels within each anatomic region that are significantly connected to the PCC seed during wake, using a low threshold ($P = 0.0001$, uncorrected). The size of the disks represents within-region connectivity, whereas thickness of lines represents between-region connectivity. During deep sleep, the posterior areas (bilateral IPC and PCC) strengthen their connectivity, whereas the connections between frontal and posterior regions are lost. See also Tables 3 and 4. MF = medial prefrontal/anterior cingulate cortex; IPl = left inferior parietal/angular gyrus; IPr = right inferior parietal/angular gyrus; PC = posterior cingulate/precuneus.

Discussion

Low-frequency fluctuations of the blood oxygen level–dependent (BOLD) signal have been observed under a wide range of physiologic conditions, including wake (4, 5, 22), light sleep (8, 15), anesthetized adults (23, 24), children (25), nonhuman primates (17), and a comatose patient (26). The present findings show that level and local structure of the low-frequency fluctuations in the BOLD signal in the regions that make up the DMN persist throughout the whole physiologic range of levels of consciousness, from wake to deep sleep; however, the strength of the correlations, and by implication the integrity of the DMN, is dynamically modulated by the level of consciousness.

It is possible that synchronization of activity in the component regions of the DMN is effected via coordinated fluctuations in membrane potentials (18, 27–30). Such coordination could be orchestrated through central regions, such as the thalamus (31) or hippocampus (32). Potential involvement of the thalamus is supported by studies that have demonstrated connections between the posterior cingulate and the laterodorsal and anteroventral thalamic nuclei in rhesus monkey (33). In addition, generalized epileptic discharges have been shown to correlate with increase in activation in thalamus and decrease in the DMN areas (34), suggesting also that thalamocortical circuits regulate activity in the DMN. Coordinated activity within the DMN may be further mediated by direct connections between the PCC/P and the other 3 nodes of the network, as demonstrated in the combined tractography and fMRI study of Greicius et al. (35). Nevertheless, full understanding of synchronization within the DMN will likely require intraoperative electrical recordings, ideally combined with fMRI.

Table 3. Between-ROI characteristics of regional BOLD signal fluctuation

ROI	MPFC	PCC	IPl	IPr
MFPC		Deep sleep: −0.11*	Deep sleep: 0.09	Deep sleep: 0.02*
PCC	Wake: 0.36		Deep sleep: 0.36	Deep sleep: 0.45
IPl	Wake: 0.01	Wake: 0.11†		Deep sleep: 0.62
IPr	Wake: .38	Wake: 0.43	Wake: 0.36†	

IPl = left inferior parietal/angular gyrus; IPr = right inferior parietal/angular gyrus. Significance set to $P < 0.05$.
*Significantly stronger during wake.
†Significantly stronger during sleep.

The finding that the MPFC is functionally decoupled from the rest of the DMN during deep sleep is consistent with the hypothesis that integrated DMN activity may reflect ongoing conscious mentation. Moreover, coherent DMN was neither found in infants (25) nor in 7–9-year-old children (36). It is possible that the absence of functional connectivity between MPFC and PCC/P in these cases could reflect differences in the nature of consciousness in children and adults. Longitudinal studies to evaluate at what point in development the DMN becomes connected will further explain this findings. Nevertheless, taken together, our findings also support the notion that waking, conscious awareness is an emergent consequence of coordinated activity in multiple brain regions (37), that it may require coherence between frontal and posterior brain regions (38), and that local cortical activity may be necessary but not sufficient to support conscious awareness [see Kanwisher's review (39)].

We have previously observed that frontal–posterior coherence in the DMN is still present in light sleep (8), and this result was recently replicated (15). In contrast, the present data indicate that during deep sleep, DMN integrity is compromised. Together, these results suggest that there is a reduction in frontoparietal correlations with increasing level (i.e., depth) of sleep, to the point of being significantly reduced at the deepest stages of sleep, when awakening threshold is the highest in humans. The differences in DMN integrity might be reflective of the reduced level of consciousness characteristic of deep sleep.

It is possible that the suspension of normal consciousness during deep sleep might be a necessary precondition for sleep-related restorative processes to occur, including changes related to homeostasis and neuronal pruning (38). The DMN decoupling we observe may provide a marker for this process. It is anticipated that further insights into the role of the DMN in consciousness will accrue from studying phenomena such as lucid dreaming (40) and sleep-state misperception (32), in which patients report the subjective experience of wakefulness during polysomnographically defined sleep.

Conclusion

Sleep-induced changes in consciousness are reflected in reduced correlations between frontal and posterior areas of the DMN during deep sleep. These changes occur in the presence of preserved activity levels in the individual network components, suggesting that it is not activity per se but rather the coherent activation of all parts within the network that leads to a conscious experience.

Table 4. Within-ROI characteristics of regional BOLD signal fluctuation

	Correlations within regions (average *r* value)		Level of fluctuations [root mean square % signal change (SE)]	
ROI	Wake	Deep sleep	Wake	Deep sleep
MPFC	0.58	0.46	0.40 (0.01)	0.31 (0.02)
PCC	0.57	0.63	0.31 (0.01)	0.41 (0.01)
IP l	0.5	0.52	0.48 (0.03)	0.43 (0.02)
IP r	0.62	0.66	0.41 (0.03)	0.41 (0.02)

Materials and Methods

Experimental Design. Simultaneous BOLD fMRI and EEG data were acquired from 18 subjects (10 female; mean age, 25.3 years, range, 21–31 years, standard deviation, 2.8 years) during deep sleep. To facilitate deep sleep in the MRI environment, the experiments were performed between 2:00 and 6:00 a.m., after 44 h of complete sleep deprivation. The experiments lasted for up to 3 h. From 5 subjects we also collected resting wake data (EEG–fMRI) before any sleep manipulation. Volunteers received monetary compensation for their participation in the study. All participants passed neurologic and audiologic evaluations and provided written informed consent, in accordance with a protocol approved by the National Institutes of Health Institutional Research Board and Walter Reed Army Institute of Research.

Data Acquisition. ***MRI acquisition.*** MRI data were acquired on a 3T scanner (GE Signa, Milwaukee, WI). For the functional scans, a 16-channel receive-only detector array (41) was used. The coil was foam-padded to restrict head motion and improve subject comfort. An additional foam mattress pad was placed on the scanner table to improve subject comfort

For BOLD fMRI, an echo planar imaging (EPI) acquisition was used that covered most of the brain and was preceded by a short EPI run that included 10 different echo times (TE), to be used as reference for correction of geometric distortions (42). Both EPI runs included 25 axial slices ($3.45 \times 3.45\text{-mm}^2$ nominal in-plane resolution, 4.5-mm thickness, 0.5-mm gap). Other parameters were repetition time (TR) = 3 s, TE = 45 ms, flip angle = 90°, and 3,600 image repetitions. To facilitate sleep, the acoustic noise generated by the EPI sequence was kept below a sound pressure level of 96 dBA by limiting the gradient slew-rate. Earplugs provided further sound attenuation. For consistency, both functional scans of each subject were performed with the same parameters.

In addition to the fMRI data, T_2-weighted and T_1-weighted anatomic images were collected to allow for image normalization to a standardized brain space based on the Montreal Neurological Institute (MNI) atlas (21). The T_1-weighted data (1-mm isotropic resolution) were acquired in a separate scan session using the product birdcage head-coil and a magnetization-prepared rapid acquisition gradient echo (MPRAGE) sequence. The T_2-weighted data consisted of fast spin echo (FSE) images collected in the same slices as the functional data and used for distortion correction and coregistration.

A pneumatic squeeze-ball, which was connected to set off a sound alarm, was provided to the volunteers. They were instructed to squeeze the ball at any point if they felt uncomfortable, wanted to interrupt the study, or wanted to communicate with the researchers. If the session was interrupted and the volunteer agreed to continue, additional T_2-weighted anatomic images were acquired to allow for correction for the potentially altered head position.

EEG and physiologic recordings. Electrical scalp recordings were made using sintered silver–silver chloride electrode caps with BrainAmp-MRplus amplifiers, and Acquire software (Brain Products). Electrodes were placed in a subset of locations of the 10–20 International System. The reference electrode was located between Fz and Cz and the ground electrode below Oz, all on the brain midline. An electrode was placed below the right eye to monitor the electrooculogram and another on the subject's back, to monitor the cardiac signal. A bipolar set of electrodes was placed on the chin to monitor submentalis muscular tone. These electrodes were connected to a bipolar amplifier

NEUROSCIENCE

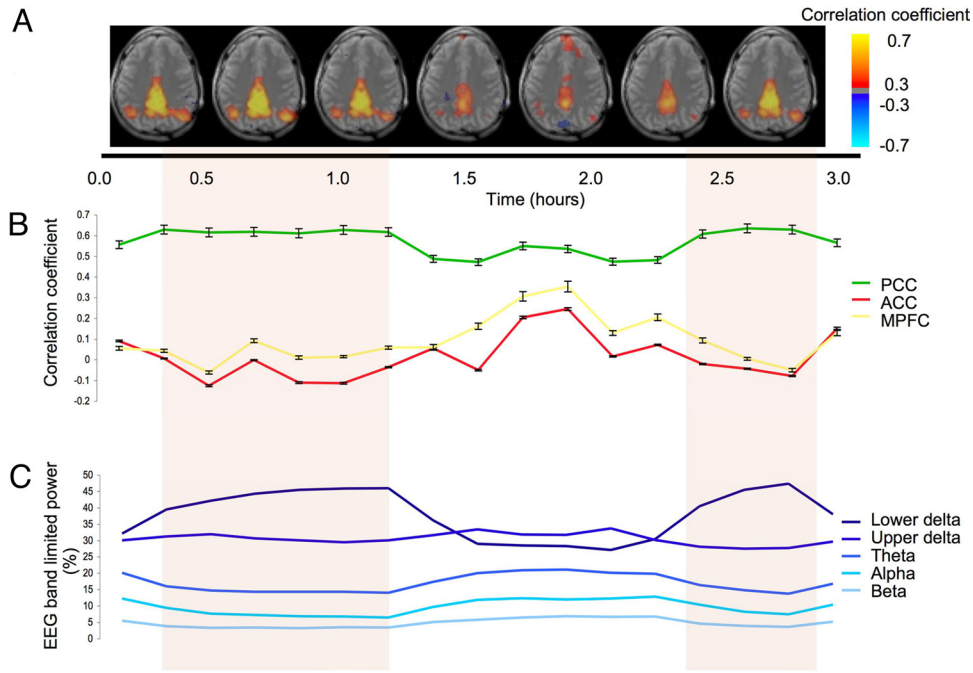

Fig. 3. Temporal evolution of connectivity within DMN at the single-subject level. (*A*) Composite single-slice maps ($Z = 25$) of correlation with seed in PCC. Each image represents the average of 2 10-min correlation maps (for full data see Fig. S3). Periods of deep sleep (indicated by colored background) coincide with a reduced involvement of frontal regions; this is confirmed by the region-based analysis shown in *B*, which shows reduced correlations with ACC and MPFC in the presence of a robust correlation within PCC. Corresponding levels of band-limited EEG activity are given in *C*, with the following definitions: lower delta: <2 Hz; upper delta: 2–4 Hz; theta: 4–8 Hz; alpha: 8–12 Hz; and beta: 12–20 Hz).

(BrainAmp-ExG-MR; Brain Products) connected to the same acquisition system as the EEG channels.

The data acquisition rate was 5 kHz, with an analog band-pass filter set to 0.016–250 Hz. Data were collected in a continuous fashion. Respiration was measured using respiratory bellows placed on the chest, and the cardiac rate was measured using a pulse oximeter placed on the left index finger. Both transducers were standard equipment on the MRI scanner. Signals from the respiratory and cardiac sensors and MRI scanner-generated trigger pulses were collected, using in-house software, at a frequency of 1 kHz.

Data Analysis. ***EEG analysis.*** Artifacts related to gradient switching and cardioballistic effects were removed using standard routines available in Analyze software (Brain Products). The data were band-pass filtered between 0.5 and 20 Hz, and manual sleep stage scoring was performed for each 12-s interval (by D.P.) using standard sleep scoring criteria (43).

Intervals of interest for analysis of deep sleep were defined as the first periods of 300 TR intervals (15 min) that had at least 30% EEG activity in the delta range (1–4 Hz) and that had been scored as stages 2 to 4 [wake, stage 1 sleep, and rapid-eye-movement (REM) sleep were excluded]. These criteria had been chosen to yield enough time points to perform correlations while avoiding the effects of arousals and REM activity.

fMRI preprocessing. Data sets were processed using custom routines written in IDL, unless otherwise indicated. First, slice-timing correction was applied to the EPI data, and these images were registered to the first image of the short EPI run that included several TE values. Both corrections were performed using SPM2 software (Wellcome Department of Cognitive Neurology, London, United Kingdom). Distortion correction was performed using the field map computed from the 10 different TEs of the short EPI run (42). This correction was necessary because of the geometric distortions that were caused by using a low bandwidth needed to decrease acoustic noise. Remaining distortion was corrected by nonlinearly deforming the EPI data to match the undistorted FSE images using AIR 5.2.5 software (44). Coregistration between subjects was performed in 2 additional steps: for each subject, the FSE images were coregistered to the MPRAGE images. Then, MPRAGE images were spatially normalized to the standard brain (MNI template). Subsequently, FSE and EP images that had been coregistered to the individual's MPRAGE images were also transformed to the standard space (both in SPM2). Physiologic noise was modeled as in Shmueli et al. (45), including RETROICOR (46), cardiac and respiration rates, and the respiration envelope. These parameters, together with a baseline regressor of third-order polynomial functions, were regressed out of the fMRI data for the 300 TRs of interest. A high-pass filter (0.005 Hz) was applied to remove any baseline drifts. These datasets were registered to a standard MNI brain ($2 \times 2 \times 2$ mm^3) for further analysis.

fMRI correlation analysis. For the default-mode correlation analysis, a seed time course was computed for each subject as the mean value of the PCC, defined anatomically according to the MNI atlas (21). These time courses were correlated with each voxel in the brain. Correlation coefficients were converted to *Z* scores using Fisher's transformation before group averaging (Fig. 1). This was performed for the wake and deep sleep data separately. A template of the default-mode network was built by thresholding ($P < 0.0001$, uncorrected) the group average results for the wake data (Fig. 1*A*). This mask was then used at individual subject level to extract the average time course for each of the main 4 components of the network (PCC/P, MPFC/ACC, and right and left IPC/AG) in both wake and deep sleep conditions. The MPFC/AC time courses were then used as seeds, and composite maps were obtained as for PCC. The composite maps are shown in Fig. S2 and the significant clusters in Table S3 and S4.

The region of interest (ROI) time courses were also correlated with each voxel within the mask to study the within-region correlation and with the other 3 time courses to study between-region correlations. The amplitude of the fluctuations at each of these regions was computed as the root mean square of the averaged time course for the region (Table 4).

We also performed a *t* test of the individual, unthresholded correlation maps of wake ($n = 5$) and deep sleep ($n = 7$) (Fig. 1*C* and Table 2).

For a single subject, signal time course was divided in consecutive intervals of 200 points (10 min). For each interval, the average time course of the PCC was correlated with whole-brain data (Fig. 3*A*). The strength of the correlation was computed by the average *r* values for the selected ROI (Fig. 3*B*), and its temporal fluctuation was correlated with that of EEG band-limited power in the lower frequencies (values computed used energy in the 1–1.33 Hz range). The correlation values for all frequencies below 2 Hz were similar. Fig. 3*C* shows the EEG spectral distribution for each interval, expressed as a percentage of the total EEG energy for that interval.

ACKNOWLEDGMENTS. This research was supported by the Intramural Research Program of the NIH, National Institute on Deafness and Other Communication Disorders and National Institute of Neurological Disorders and Stroke, and WRAIR.

1. Raichle ME (1981) Measurement of local cerebral blood flow and metabolism in man with positron emission tomography. *Fed Proc* 40:2331–2334.
2. Ogawa S, et al. (1993) Functional brain mapping by blood oxygenation level-dependent contrast magnetic resonance imaging. A comparison of signal characteristics with a biophysical model. *Biophys J* 64:803–812.
3. Beckmann CF, DeLuca M, Devlin JT, Smith SM (2005) Investigations into resting-state connectivity using independent component analysis. *Philos Trans R Soc Lond B Biol Sci* 360:1001–1013.
4. Biswal B, Yetkin FZ, Haughton VM, Hyde JS (1995) Functional connectivity in the motor cortex of resting human brain using echo-planar MRI. *Magn Reson Med* 34:537–541.
5. Cordes D, et al. (2000) Mapping functionally related regions of brain with functional connectivity MR imaging. *AJNR Am J Neuroradiol* 21:1636–1644.
6. Fox MD, Raichle ME (2007) Spontaneous fluctuations in brain activity observed with functional magnetic resonance imaging. *Nat Rev Neurosci* 8:700–711.
7. Greicius MD, Krasnow B, Reiss AL, Menon V (2003) Functional connectivity in the resting brain: A network analysis of the default mode hypothesis. *Proc Natl Acad Sci USA* 100:253–258.
8. Horovitz SG, et al. (2008) Low frequency BOLD fluctuations during resting wakefulness and light sleep: A simultaneous EEG-fMRI study. *Hum Brain Mapp* 29:671–682.
9. Arieli A, Shoham D, Hildesheim R, Grinvald A (1995) Coherent spatiotemporal patterns of ongoing activity revealed by real-time optical imaging coupled with single-unit recording in the cat visual cortex. *J Neurophysiol* 73:2072–2093.
10. Nir Y, Dinstein I, Malach R, Heeger DJ (2008) BOLD and spiking activity. *Nat Neurosci* 11:523–524, author reply 524.
11. Shmuel A, Leopold DA (2008) Neuronal correlates of spontaneous fluctuations in fMRI signals in monkey visual cortex: Implications for functional connectivity at rest. *Hum Brain Mapp* 29:751–761.
12. Mazoyer B, et al. (2001) Cortical networks for working memory and executive functions sustain the conscious resting state in man. *Brain Res Bull* 54:287–298.
13. Raichle ME, et al. (2001) A default mode of brain function. *Proc Natl Acad Sci USA* 98:676–682.
14. Gusnard DA, Raichle ME (2001) Searching for a baseline: Functional imaging and the resting human brain. *Nat Rev Neurosci* 2:685–694.
15. Larson-Prior LJ, et al. (2009) Cortical network functional connectivity in the descent to sleep. *Proc Natl Acad Sci USA* 106:4489–4494.
16. Hobson JA, Pace-Schott EF (2002) The cognitive neuroscience of sleep: Neuronal systems, consciousness and learning. *Nat Rev Neurosci* 3:679–693.
17. Vincent JL, et al. (2007) Intrinsic functional architecture in the anaesthetized monkey brain. *Nature* 447:83–86.
18. Rechtschaffen A, Hauri P, Zeitlin M (1966) Auditory awakening thresholds in REM and NREM sleep stages. *Percept Mot Skills* 22:927–942.
19. Zeman A (2001) Consciousness. *Brain* 124(Pt 7):1263–1289.
20. Laureys S (2005) The neural correlate of (un)awareness: Lessons from the vegetative state. *Trends Cogn Sci* 9:556–559.
21. Tzourio-Mazoyer N, et al. (2002) Automated anatomical labeling of activations in SPM using a macroscopic anatomical parcellation of the MNI MRI single-subject brain. *Neuroimage* 15:273–289.
22. Fransson P (2005) Spontaneous low-frequency BOLD signal fluctuations: An fMRI investigation of the resting-state default mode of brain function hypothesis. *Hum Brain Mapp* 26:15–29.
23. Greicius MD, et al. (2008) Persistent default-mode network connectivity during light sedation. *Hum Brain Mapp* 29:839–847.
24. Kiviniemi VJ, et al. (2005) Midazolam sedation increases fluctuation and synchrony of the resting brain BOLD signal. *Magn Reson Imaging* 23:531–537.
25. Fransson P, et al. (2007) Resting-state networks in the infant brain. *Proc Natl Acad Sci USA* 104:15531–15536.
26. Boly M, et al. (2008) Intrinsic brain activity in altered states of consciousness: How conscious is the default mode of brain function? *Ann N Y Acad Sci* 1129:119–129.
27. Bressler SL, Coppola R, Nakamura R (1993) Episodic multiregional cortical coherence at multiple frequencies during visual task performance. *Nature* 366:153–156.
28. Gray CM, Singer W (1989) Stimulus-specific neuronal oscillations in orientation columns of cat visual cortex. *Proc Natl Acad Sci USA* 86:1698–1702.
29. Massimini M, Huber R, Ferrarelli F, Hill S, Tononi G (2004) The sleep slow oscillation as a traveling wave. *J Neurosci* 24:6862–6870.
30. Roelfsema PR, Engel AK, Konig P, Singer W (1997) Visuomotor integration is associated with zero time-lag synchronization among cortical areas. *Nature* 385:157–161.
31. Steriade M, McCormick DA, Sejnowski TJ (1993) Thalamocortical oscillations in the sleeping and aroused brain. *Science* 262:679–685.
32. Itskov V, Pastalkova E, Mizuseki K, Buzsaki G, Harris KD (2008) Theta-mediated dynamics of spatial information in hippocampus. *J Neurosci* 28:5959–5964.
33. Morris R, Petrides M, Pandya DN (1999) Architecture and connections of retrosplenial area 30 in the rhesus monkey (*Macaca mulatta*). *Eur J Neurosci* 11:2506–2518.
34. Gotman J, et al. (2005) Generalized epileptic discharges show thalamocortical activation and suspension of the default state of the brain. *Proc Natl Acad Sci USA* 102:15236–15240.
35. Greicius MD, Supekar K, Menon V, Dougherty RF (2009) Resting-state functional connectivity reflects structural connectivity in the default mode network. *Cereb Cortex* 19:72–78.
36. Fair DA, et al. (2008) The maturing architecture of the brain's default network. *Proc Natl Acad Sci USA* 105:4028–4032.
37. Baars BJ (2005) Global workspace theory of consciousness: Toward a cognitive neuroscience of human experience. *Prog Brain Res* 150:45–53.
38. Tononi G, Koch C (2008) The neural correlates of consciousness: An update. *Ann N Y Acad Sci* 1124:239–261.
39. Kanwisher N (2001) Neural events and perceptual awareness. *Cognition* 79:89–113.
40. Eeden FV (1913) A study of dreams. *Proc Soc Psychic Res* 26:431–461.
41. de Zwart JA, et al. (2004) Signal-to-noise ratio and parallel imaging performance of a 16-channel receive-only brain coil array at 3.0 Tesla. *Magn Reson Med* 51:22–26.
42. Jezzard P, Balaban RS (1995) Correction for geometric distortion in echo planar images from B0 field variations. *Magn Reson Med* 34:65–73.
43. Rechtschaffen A, Kales A, eds (1968) *A Manual of Standardized Terminology, Techniques and Scoring System for Sleep Stages of Human Subjects* (U. S. National Institute of Neurological Diseases and Blindness, Neurological Information Network, Bethesda, MD).
44. Woods RP, Grafton ST, Holmes CJ, Cherry SR, Mazziotta JC (1998) Automated image registration: I. General methods and intrasubject, intramodality validation. *J Comput Assist Tomogr* 22:139–152.
45. Shmueli K, et al. (2007) Low-frequency fluctuations in the cardiac rate as a source of variance in the resting-state fMRI BOLD signal. *Neuroimage* 38:306–320.
46. Glover GH, Li TQ, Ress D (2000) Image-based method for retrospective correction of physiological motion effects in fMRI: RETROICOR. *Magn Reson Med* 44:162–167.